International Journal of Naval Architecture and Ocean Engineering 11 (2019) 679–687

Contents lists available at ScienceDirect

International Journal of Naval Architecture and Ocean Engineering

journal homepage: http://www.journals.elsevier.com/international-journal-of-naval-architecture-and-ocean-engineering/

Autonomous swimming technology for an AUV operating in the underwater jacket structure environment

Ji-Hong Li*, Daegil Park, Geonhui Ki

Marine Robotics R&D Division, Korea Institute of Robot and Convergence, Jigok-Ro 39, Nam-Gu, Pohang, 37666, Republic of Korea

ARTICLE INFO

Article history:
Received 16 October 2018
Received in revised form
20 November 2018
Accepted 19 February 2019
Available online 26 February 2019

Keywords:
Autonomous Underwater Vehicle (AUV)
Autonomous navigation
Underwater localization
Occupancy Grid Map (OGM)
Obstacle detection
Path planning

ABSTRACT

This paper presents the autonomous swimming technology developed for an Autonomous Underwater Vehicle (AUV) operating in the underwater jacket structure environment. To prevent the position divergence of the inertial navigation system constructed for the primary navigation solution for the vehicle, we've developed kinds of marker-recognition based underwater localization methods using both of optical and acoustic cameras. However, these two methods all require the artificial markers to be located near to the cameras mounted on the vehicle. Therefore, in the case of the vehicle far away from the structure where the markers are usually mounted on, we may need alternative position-aiding solution to guarantee the navigation accuracy. For this purpose, we develop a sonar image processing based underwater localization method using a Forward Looking Sonar (FLS) mounted in front of the vehicle. The primary purpose of this FLS is to detect the obstacles in front of the vehicle. According to the detected obstacle(s), we apply an Occupancy Grid Map (OGM) based path planning algorithm to derive an obstacle collision-free reference path. Experimental studies are carried out in the water tank and also in the Pohang Yeongilman port sea environment to demonstrate the effectiveness of the proposed autonomous swimming technology.

1. Introduction

In the past decades, autonomous navigation has been one of the most hot research topic in the robotics community (Laugier and Chatila, 2007). Recently, due to the rapid development of AI technology (Russell and Norvig, 2009), quite number of car makers, as well as leading companies in the industries such as Google, Apple, and Uber, have presented various self-driving technologies. Since 2009, Google self-driving car has racked up 5 million self-driven miles. However, in the case of underwater vehicles, autonomous navigation research activities still focus on the some of basic items, such as how to improve the localization accuracy, and how to detect the obstacle and further to avoid it, etc. In this paper, we propose a sonar image processing based underwater localization method and obstacle detection and path planning method both using FLS mounted in front of the vehicle.

In the December 2012, the Korea Institute of Robot and Convergence (KIRO) launched a project funded by the Ministry of Trade, Industry and Energy (MOTIE) in South Korea. The main purpose of this project is to develop an autonomous swimming technology for an AUV operating in the underwater jacket structure environment. For the vehicle's underwater navigation, we've constructed a strapdown inertial navigation system (Tittertonm and Weston, 1997; Farrell and Barth, 1998) using the Inertial Measurement Unit (IMU), DVL, ARS, and depth sensor (Li et al., 2012). And to prevent the position divergence of this hybrid inertial navigation system, two of marker-recognition based underwater localization methods, one is using camera vision (Jung et al., 2017) and the other one using acoustic camera (Lee et al., 2017), have been developed for the purpose of position aiding. In order to acquire the clear image to recognize the markers which are usually attached on the structure(s), these two methods all require the vehicle to approach to the markers closely. Usually, in the sea environment around the korean peninsula, the visibility range is less than 4 5 m, and in the case of high turbidity such as in the western sea environment, this range is less than 1 m. If the vehicle is far away from the structure, we could not use the above mentioned localization methods and might need an alternative one to guarantee the navigation accuracy. For our test-bed AUV (Li et al., 2017), there is a FLS

* Corresponding author.
E-mail address: jhli5@kiro.re.kr (J.-H. Li).
Peer review under responsibility of Society of Naval Architects of Korea.

https://doi.org/10.1016/j.ijnaoe.2019.02.002

(BlueView Technologies Inc., 2013) whose object detection range can be up to 100 m, mounted in front of the vehicle. If the jacket structure's pose (position and orientation) information is known *in priori*, then we can estimate the vehicle's current navigation error through certain sonar image processing method (Li et al., 2017, 2018). Given current navigation result which usually includes the accumulated position error, we can estimated the jacket structure's position and orientation relative to the sonar head, and even further can construct a sort of virtual sonar image. Through comparing this virtual image with the sonar raw image, reversely we can abstract the error component in the current navigation result. This navigation error further can be used to correct the next step of navigation result.

As mentioned before, the primary purpose of FLS is to detect the obstacles in real time. Given obstacle(s) sonar raw image, we can abstract the candidate objects through a series of image processes. And those candidates located outside of previously known structures around the vehicle (for examples, jacket structure, water tank walls, and breakwaters in the sea environment) are considered as the obstacles. Given detected obstacle and structure information, we apply a sort of OGM based path planning method (Latombe, 1991; Thurn et al., 1997) to find out a collision-free reference path approaching to the target point.

To demonstrate the effectiveness of proposed FLS image processing based underwater localization method and OGM based path planning method, we carry out various experimental studies both in the water tank environment and in the Pohang Yeongilman port sea environment. During the sea test, we find that the test-bed vehicle can fully autonomously swim in and swim out of the test-bed jacket structure and recognize all of 20 camera vision markers attached on the structure.

The remainder of this paper is organized as follows. Hybrid inertial navigation system which is constructed as the primary navigation tool for the vehicle is introduced in Section 2, and sonar image processing based underwater localization method is proposed in the following section. Series of sonar image processing based obstacle detecting method and OGM based path planning algorithm are discussed in Section 4, and Section 5 presents the sea experimental results. Finally, a brief conclusion is made in Section 6.

2. Hybrid inertial navigation system

An inertial navigation system combined with DVL, ARS, and depth sensor is constructed as the primary navigation system for out test-bed AUV, as seen in Fig. 1. Two position-aiding methods are applied to prevent the position divergence of inertial navigation system: one is optical camera vision based underwater localization method (Jung et al., 2017), where the markers are attached on the jacket structure, and the other one is an acoustic camera vision based localization method (Lee et al., 2017) with the markers installed on the seafloor around the jacket structure.

2.1. Navigation error state equation

Constructed navigation filter state equation is as follows, which is the same as in Li et al. (2012),

$$\dot{X}(t) = F(t)X(t) + G(t)\omega(t), \tag{1}$$

where $X = [\delta\lambda, \delta\Phi, \delta h, \delta v_N, \delta v_E, \delta v_D, \varepsilon_N, \varepsilon_E, \varepsilon_D, b_{ax}, b_{ay}, b_{az}, b_p, b_q, b_r]^T$. For all of other matrix and parameter definitions and notations, refer to Li et al. (2012).

Compare to the previous similar work done by Lee et al. (2007), in this paper, we do not include the bias terms in the DVL, ARS and depth sensor outputs into the state vector X. Since lack of proper dynamics of these bias terms in the vehicle's geodetic error dynamics, in practice, we found that it is difficult to properly estimate these bias terms using Kalman filter. Instead, the value of these terms can be roughly pre-determined through proper careful calibrations in practice.

2.2. Navigation error measurement equation

As mentioned before, a strapdown inertial navigation system combined with DVL, ARS, and depth sensor is constructed as the primary navigation system. And two additional underwater localization methods, each using optical and acoustic camera visions, are applied to provide position-aiding. Therefore, the measurements error equations can be expressed as

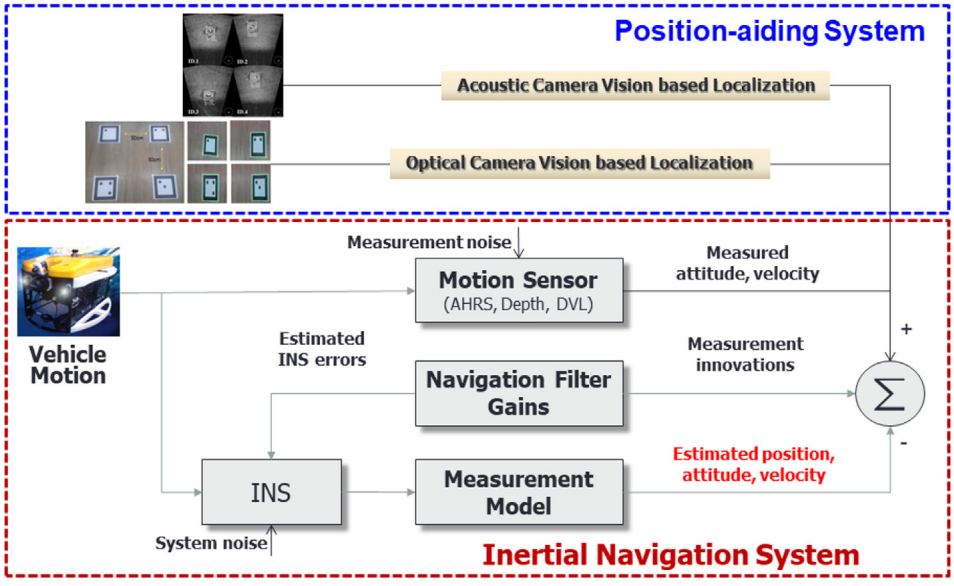

Fig. 1. Hybrid INS combined with two of camera vision based position-aiding methods.

$$\widehat{\lambda} - \lambda_{m\_i} = (\lambda - \delta\lambda) - \left(\lambda - \upsilon_{\lambda_i}\right) = -\delta\lambda + \upsilon_{\lambda_i}, \tag{2}$$

$$\widehat{\Phi} - \Phi_{m\_i} = (\Phi - \delta\Phi) - \left(\Phi - \upsilon_{\Phi_i}\right) = -\delta\Phi + \upsilon_{\Phi_i}, \tag{3}$$

$$\widehat{h} - h_m = (h - \delta h) - (h - \upsilon_h) = -\delta h + \upsilon_h, \tag{4}$$

$$\begin{aligned}\widehat{V}^n - V_m^n &= (V^n - \delta V^n) - \widehat{C}_b^n\left(V^b - \upsilon_V\right)\\ &= (V^n - \delta V^n) - (I - P)C_b^n\left(V^b - \upsilon_V\right)\\ &= -\delta V^n + PC_b^n V_m^b + \widehat{C}_b^n \upsilon_V,\end{aligned} \tag{5}$$

$$\widehat{\varphi} - \varphi_m = (\varphi - \rho) - \left(\varphi - \upsilon_\varphi\right) = -\rho + \upsilon_\varphi, \tag{6}$$

where $\widehat{(\cdot)}$ means the estimation value, subscript m denotes the measurement value, superscript n, b each means the value defined in the navigation frame (NED frame) and body-fixed frame, δ means state error; λ and Φ denote longitude and latitude, and υ_λ and υ_Φ denote Gaussian white noises with $\upsilon_\lambda(\cdot) \sim N(0, R_\lambda(\cdot))$ and $\upsilon_\Phi(\cdot) \sim N(0, R_\Phi(\cdot))$, with $i = \{optical, acoustic\}$. For more details and other notations, refer to Li et al. (2012).

It is necessary to mention that in Eq. (6), the attitude vector φ is defined as $\varphi = [\phi, \theta]^T$ instead of $[\phi, \theta, \psi]^T$, and corresponding attitude error vector is taken as $\rho = [\varepsilon_N, \varepsilon_E]^T$. In most of practical applications, the ARS sensors are usually surrounded by various electric and electronics devices, and these devices are usually cause the earth's magnetic field distortion around the ARS after they are powered on. Unfortunately, most of these ARS sensors are using built-in magnetometer to aid their heading measurements, and therefore these uncorrect heading measurement might cause critical problem for navigation filter. Under this consideration, in this paper, the ARS heading measurement is not used in the measurement update of our navigation filter.

Consequently, the navigation error measurement equation is as follows,

$$Y(t) = C(t)X(t) + H(t)\upsilon(t), \tag{7}$$

where matrix $C(t)$ and $H(t)$ can be expressed as

$$\begin{aligned}C &= \begin{bmatrix} -1 & 0 & 0_{1\times7} & 0_{1\times6} \\ -1 & 0 & 0_{1\times7} & 0_{1\times6} \\ 0 & -1 & 0_{1\times7} & 0_{1\times6} \\ 0 & -1 & 0_{1\times7} & 0_{1\times6} \\ 0_{1\times2} & -1 & 0_{1\times6} & 0_{1\times6} \\ 0_{3\times3} & -I_{3\times3} & CV_{3\times3} & 0_{3\times6} \\ 0_{2\times3} & 0_{2\times3} & -I_{2\times2} & 0_{2\times7} \end{bmatrix}, H\\ &= \begin{bmatrix} 1 & 0 & 0_{1\times8} \\ 1 & 0 & 0_{1\times8} \\ 0 & 1 & 0_{1\times8} \\ 0 & 1 & 0_{1\times8} \\ 0_{1\times2} & 1 & 0_{1\times7} \\ 0_{3\times5} & \widehat{C}_b^n & 0_{3\times2} \\ 0_{2\times5} & 0_{2\times3} & I_{2\times2} \end{bmatrix},\end{aligned}$$

where

$$CV = \begin{bmatrix} 0 & -V_m^n(3) & V_m^n(2) \\ V_m^n(3) & 0 & -V_m^n(1) \\ -V_m^n(2) & V_m^n(1) & 0 \end{bmatrix},$$

with $V_m^n = C_b^n V_m^b$. In (7), Gaussian noise vector $\upsilon = [\upsilon_{\lambda_{optical}}, \upsilon_{\lambda_{acoustic}}, \upsilon_{\Phi_{optical}}, \upsilon_{\Phi_{acoustic}}, \upsilon_h, \upsilon_V^T, \upsilon_\varphi^T]^T \sim N(0, R)$.

2.3. Construction of discrete-time navigation filter

Discrete-time navigation filter can be constructed as follows as in Li et al. (2012),

$$X_{k+1} = F_k^s X_k + \omega_k, \tag{8}$$

$$Y_k = C_k^s X_k + \upsilon_k, \tag{9}$$

where $C_k^s = C(t)$ and

$$F_k^s = e^{F\delta t} \approx I + F\delta t + \frac{F^2}{2!}\delta t^2 + \frac{F^3}{3!}\delta t^3, \tag{10}$$

and $\omega_k \sim N(0, Q^s)$ with

$$\begin{aligned}Q^s \approx GQG^T\delta t + \frac{FGQG^T + GQG^TF^T}{2!}\delta t^2\\ + \frac{F^2GQG^T + 2FGQG^TF^T + GQG^T(F^T)^2}{3!}\delta t^3,\end{aligned} \tag{11}$$

and $\upsilon_k \sim N(0, R^s)$ with $R^s = (HRH^T)/\delta t$.

At each time step, the filter is updated as follows (Lewis, 1986),

Time update

$$P_{k+1}^- = F_k^s P_k (F_k^s)^T + Q^s \tag{12}$$

$$\widehat{x}_{k+1}^- = F_k^s \widehat{x}_k \tag{13}$$

Measurement update

$$P_{k+1} = P_{k+1}^- - P_{k+1}^-(C_k^s)^T\left[C_k^s P_{k+1}^-(C_k^s)^T + R^s\right]^{-1} C_k^s P_{k+1}^- \tag{14}$$

$$\widehat{x}_{k+1} = \widehat{x}_{k+1}^- + P_{k+1}(C_k^s)^T(R^s)^{-1}\left(Y_{k+1} - C_k^s\widehat{x}_{k+1}^-\right) \tag{15}$$

3. Sonar image processing based underwater localization

Consider the case where the vehicle is swimming in the area with the jacket structure located in the view range of FLS mounted in front of the vehicle. If the structure's position and orientation information are known *in priori*, then according to the vehicle's previous step of navigation result which usually includes a sort of accumulated error, we can construct a kind of virtual sonar image, see Fig. 2(a). Through comparing this virtual image with the sonar raw image as shown in Fig. 2(b), reversely, we can abstract the error terms in the previous step of navigation result. These abstracted error terms further can be applied to aid the vehicle's current step of position update (Li et al., 2018). And this is the main idea of underwater localization method proposed in this paper using sonar image processes.

3.1. Two images matching algorithm

For the hybrid inertial navigation system constructed for our test-bed vehicle, we are confident of its yaw angle estimation. Therefore, during the images matching, we only consider the image shifting along both of row and column directions without any of rotation. Images matching algorithm is as follows as in Li et al. (2017),

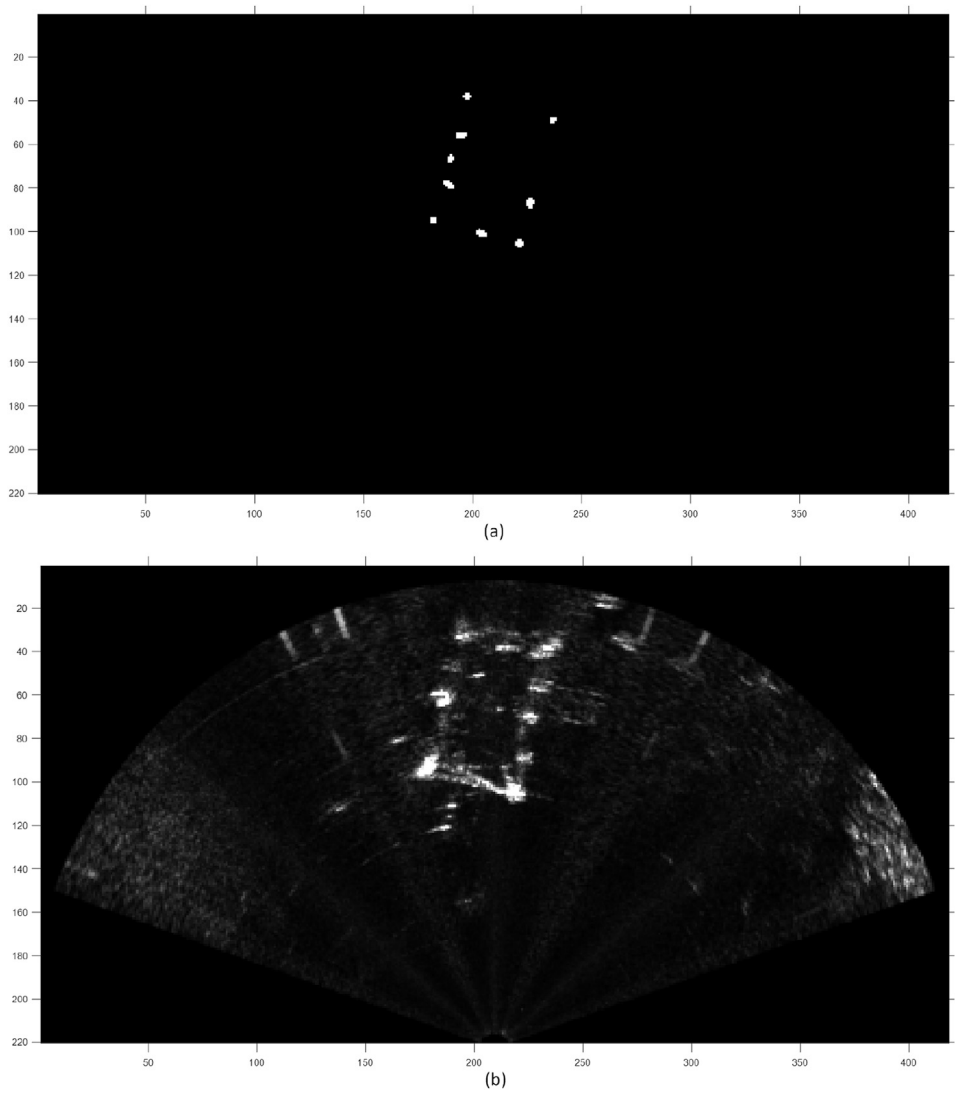

Fig. 2. Two of sonar images: (a) is the constructed structure virtual image $G_e^{n\times m}$, and (b) is the sonar raw image $G_r^{n\times m}$.

$$
\begin{gathered}
for\ (k=-C_N;\ k\le C_N;\ k++)\\
for\ (l=-C_E;\ l\le C_E;\ l++)\\
Shift\ G_e^{n\times m}\ in\ the\ row\ direction\ with\ k\ grids,\ and\ in\ the\\
columne\ direction\ with\ l\ grids.\\
Then,\ calculate\ the\ correlation\ value\ between\ G_e^{n\times m}\\
and\ G_r^{n\times m}\ as\ follows,\\
Corr_{k,l}=\sum_{i=1,\,j=1}^{i=n,\,j=m} M_{i,j}^{G_e^{n\times m}}\cdot M_{i,j}^{G_r^{n\times m}}\\
end\\
end\\
Search\ the\ maximum\ value\ of\ Corr_{k,l}\ and\ corresponding\ shift\\
corresponding\ shift\ value\ (k,l).
\end{gathered}
$$

where C_N, C_E are design parameters, and $M_{i,j}$ denotes the magnitude of image bright intensity for each of (i,j) grid.

3.2. Position aiding

Using calculated shifting value (k,l), the vehicle's current step of position can be corrected as follows (Li et al., 2018),

$$x_{correct} = x_{current} + k\cdot R_{res}, \tag{16}$$

$$y_{correct} = y_{current} + l\cdot R_{res}, \tag{17}$$

where R_{res} is the image resolution.

In practice, while getting the sonar raw image as seen in Fig. 2-(b), we usually reduce the image resolution (or increase the grid size) in order to fast the image matching process speed.

Position measurement equation for the navigation filter is as follows,

$$\begin{bmatrix}\widehat{x}\\ \widehat{y}\end{bmatrix}-\begin{bmatrix}x_{correct}\\ y_{correct}\end{bmatrix}=\begin{bmatrix}-R_N\cos\psi_0 & -R_E\sin\psi_0\\ R_N\sin\psi_0 & -R_E\cos\psi_0\end{bmatrix}\left(\begin{bmatrix}\delta\lambda\\ \delta\Phi\end{bmatrix}-\begin{bmatrix}\upsilon_\lambda\\ \upsilon_\Phi\end{bmatrix}\right), \tag{18}$$

where (x,y) is the horizontal position in the local frame; ψ_0 denotes the local frame rotation angle from NED frame; R_N and R_E are two of the earth radius parameters (Tittertonm and Weston, 1997); $\upsilon_\lambda \sim N(0, R_{\upsilon_\lambda})$ and $\upsilon_\Phi \sim N(0, R_{\upsilon_\Phi})$ where R_{υ_λ} and R_{υ_Φ} are tuning parameters.

4. OGM based path planning algorithm

OGM is a sort of grid map where each grid is assigned with a unique value, which is usually calculated through certain criteria function (Latombe, 1991; Thurn et al., 1997). In this paper, we apply a potential function to calculate the unique value of each grid. Given a OGM, the search algorithm for this map is simple that at each step, among its unsearched neighboring grids, we select the one assigned with the smallest potential value.

4.1. Obstacle detection

As mentioned before, the primary purpose of FLS mounted in front of the test-bed vehicle is to detect the obstacle in real time. Obstacle detection scenario is as shown in Fig. 3. At each time step, we can get a ping of sonar raw image (BlueView Technologies Inc., 2013), as seen in Fig. 3(a). In order to speed up the detection algorithm, or actually the map searching algorithm, we may have to reduce the image resolution. In fact, the FLS for the test-bed vehicle has the 2 cm of resolution. And in most of practical applications, we do not need this kind of accuracy. In this paper, the resolution or same as grid size is set to five times to its original one as shown in Fig. 3(b). Using this resolution-reduced image, through proper coordinate transformation from NED frame to local navigation frame (in this case, the local frame is a water tank environment with the dimension of 12(L)x8(W)x6(D)m), we can get the sonar image fit to this local frame as seen in Fig. 3(c). Further using properly designed threshold parameter, we get the filtered image as Fig. 3(d). Using this image, we apply the following search algorithm: *We search the grids group where each grid's intensity value larger than the threshold and each grid is connected to each other. If the grids number in a group is larger than certain design parameter, then this grids group is considered as an obstacle, as seen in* Fig. 3(e).

It is notable that this kind of obstacle detection algorithm can be easily applicable to other local frames where the local environmental geometric information is known *in priori*.

4.2. OGM construction

For a given geometric information of the vehicle's operating environment including the artificial underwater structure's dimension, position, and orientation, and breakwaters orientation, etc., we can construct a 3D grids pile for this field. The grid size can be chosen according to the practical mission requirements. And the map construction procedure is as follows,

- At first, the grids which are occupied by the artificial structures and sea floor (at this step, we assume that there is not any obstacle detected yet) are assigned with value 1, and the remainder of grids are all set to 0 value.
- Given the target point (or grid), all of grids with 0 value are assigned by the unique values according to the following potential function (Li et al., 2018)

$$U(q) = U_{att}(q) + U_{re}(q) = c_{att} r_{tp}^{a} + \sum_{i=1}^{n} c_{rep} r_i^{-b}, \tag{19}$$

where U_{att} denotes the attractive potential and U_{rep} is repulsive one, r_{tp} is the distance between current grid to the target grid and r_i means the range between current grid to the grid with the value of 1, c_{att}, c_{rep}, a and b are design parameters, and n denotes the grids number with the value of 1.

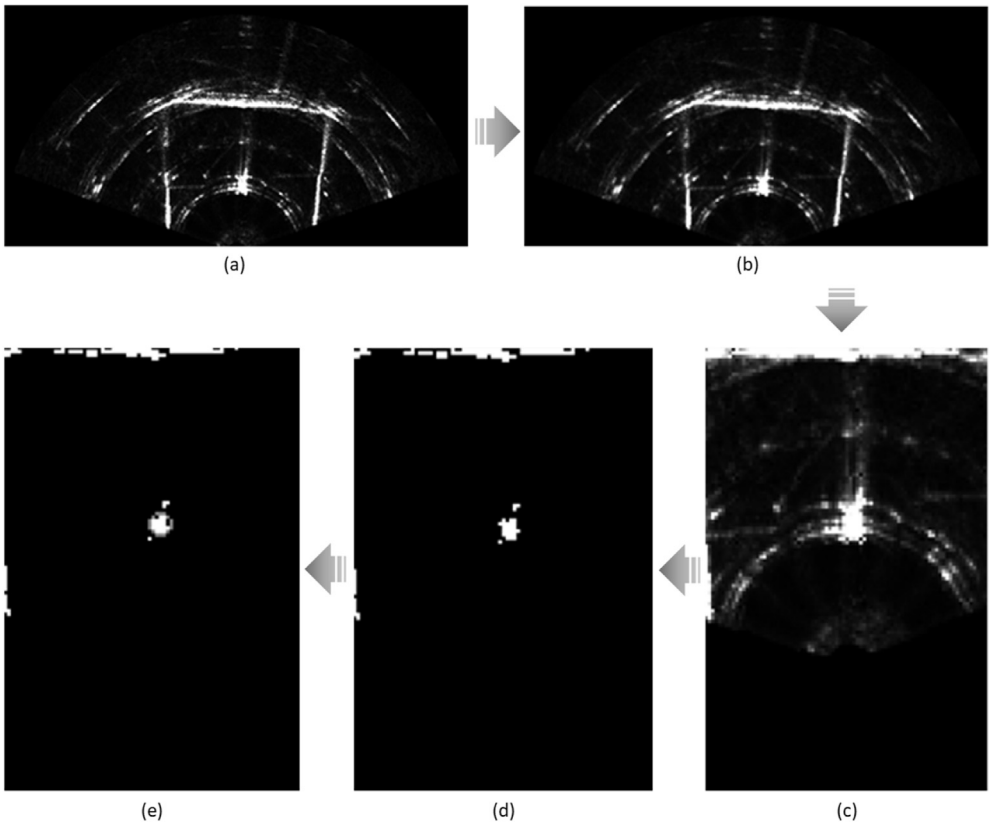

Fig. 3. Obstacle detection scenario: (a) FLS raw image, (b) resolution reduced image, (c) image transfer to the local navigation frame, (d) filtered image, (e) detected obstacle.

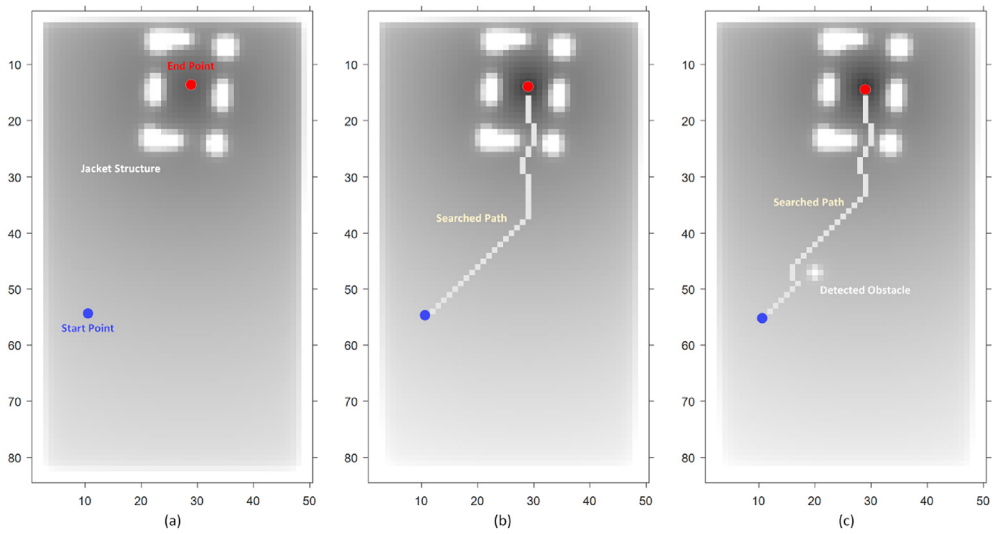

Fig. 4. OGM construction and path planning: (a) initial OGM construction, (b) path planning in the initial OGM, (c) obstacle avoidance.

- After all of these 0 value grids are reset by the unique values, the initial OGM is completed as seen in Fig. 4(a).

During the OGM construction, how to select the map grid size becomes very important in practical applications. If the grid dimension is chosen too large, then it is difficult to distinguish the artificial structures and therefore in some cases, it would be impossible to find out a path even if there is one such that the vehicle can swim through the structure. On the other hand, if grid size is too small, then map searching time will be exponentially increasing.

4.3. Path planning

Using constructed OGM, we can easily find out a path approaching to the target point by applying the following search algorithm: *At each step or grid, among its 26 neighboring grids, search the unsearched grids, and choice the grid with the minimum of* $U(q)$.

Since we use Eq. (20) to assign unique value to a grid, it is quite possible for the vehicle to fall in a local minimum grid (Latombe, 1991; Thurn et al., 1997) while searching the grid map. In this case, we modify the parameters c_{att} and c_{rep} in (20) and re-search the path. And, this process will be repeated until find out a path approaching to the target point.

While swimming along the searched path as seen in Fig. 4(b), if the vehicle detect the obstacle(s), then it will reset all of these none 1 value of grids using (20), and all of grids occupied by obstacle(s) will be assigned with 1 value. Using this updated OGM, the vehicle will search another suboptimal path to approach to the target point without collision with obstacle(s), see Fig. 4(c).

5. Sea experimental studies

From November in 2017 to January in 2018, we carried out a series of tests in the Yeongilman port sea environment in the Pohang city in South Korea to demonstrate the effectiveness of our developed autonomous swimming technology.

5.1. Experiment setup

During the project, a small-scaled jacket structure model was manufactured as shown in Fig. 5. At first, this model was installed in a water tank environment and in October 2017, moved to and installed on the about 17 m depth of sea floor in the Pohang Yeongilman port. There are total of 20 vision markers mounted on the structure as seen in Fig. 5, and two of acoustic camera markers are installed on the sea floor near the structure. After installation of structure, two divers dived into the field and measured the structure's position and orientation relative to the two orthogonal breakwaters, which are chosen as the X and Y axes of the local navigation frame, see Fig. 5. The origin of this local frame is located in the NED reference frame at $N : 36.048748^o$, $E : 129.382035^o$, and the local frame orientation is $\psi = 270^o$.

In each test, at first, the vehicle is operated manually and oriented to parallel to one of two breakwater walls (X or Y axis in the local frame). This operation is carried out by operator through monitoring the FLS real time image on the surface unit. By dong so, we can get the vehicle's rough initial heading information. This is a sort of initial alignment of constructed inertial navigation system. On the surface, GPS is used for position-aiding.

5.2. Autonomous swimming test

The test scenario is as follows.

- After its rough heading initialization, the vehicle will receive an *AutoSwimming_Mission_Start* command from the surface unit. At first, the vehicle will swim away about 10 m from both of two breakwaters on the surface. This is because there are lots of rocks and concrete structures on the sea floor near the breakwater, and this kind of bumpy sea floor usually cause significant measurement noise on the DVL output and sometimes can even cause the DVL dropout (Fairfield et al., 2008). At the certain surface point away from the breakwaters, the vehicle starts its hybrid inertial navigation algorithm and dives into previously set depth.
- After diving to this previously set depth, the vehicle will swim to the point in front of the previously pointed certain optical camera vision marker. Two of previously mentioned acoustic camera vision markers are installed on the sea floor near to this target point. Therefore, during this swimming to the point in front of the camera marker, there is not any artificial marker available for the vehicle to acquire position

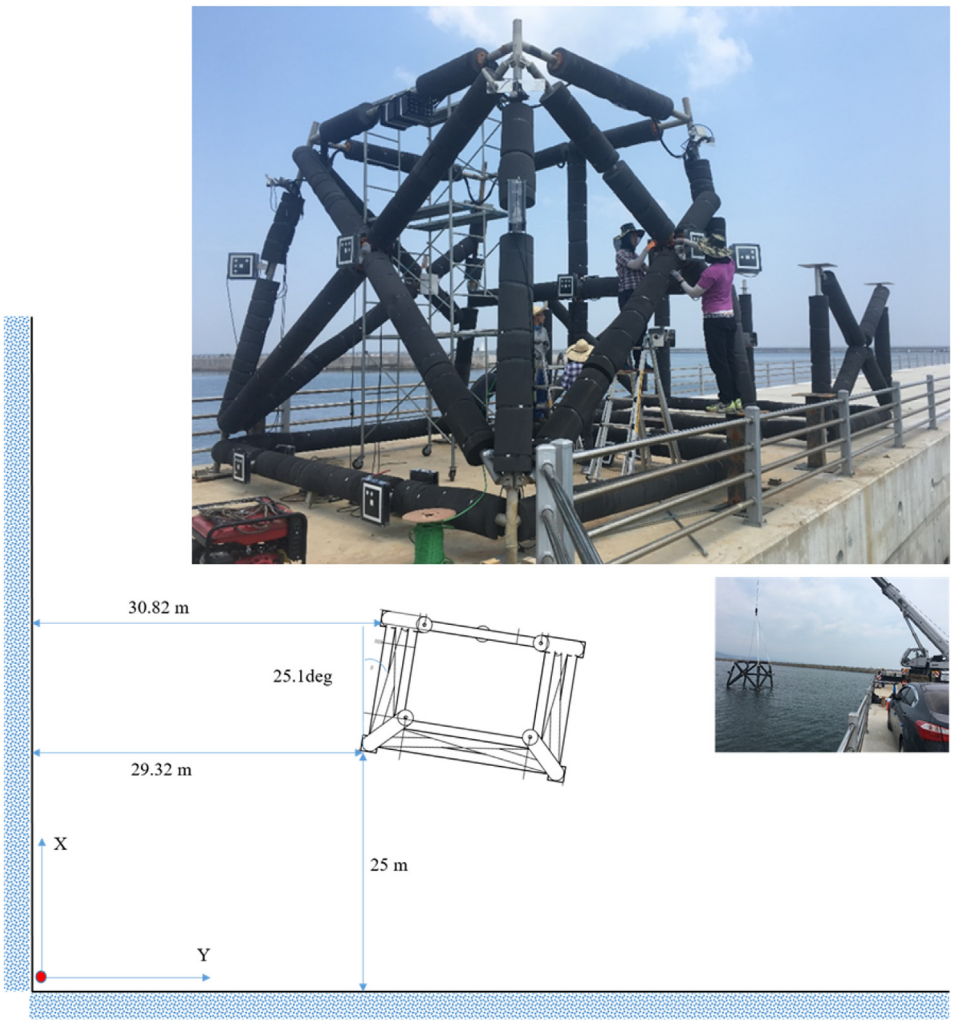

Fig. 5. Scaled jacket structure model preparation and sea test setup.

aiding. And, FLS image processing based localization method proposed in this paper is used to provide position aiding to the inertial navigation system so that can prevent the position's far divergence.

- In front of the previously pointed vision marker, the vehicle will recognize the marker and get the position aiding. After that, the vehicle will swim around and in/out of the jacket structure and recognize a series of vision markers mounted on the structure. The number and sequence of markers are transmitted to the vehicle on the surface before mission start command.
- After finishing the recognition of the given series of vision markers, the vehicle will return to the certain end point while keeping its depth. During this swimming, if the vehicle find out obstacle(s), then it will re-plan a collision-free path and swim along this new path.

All of sensors raw data including camera video clips as well as all algorithm results from navigation, obstacle detection, path planning, etc. are logged on the vehicle computer for the purpose of post analysis.

5.3. Experiments result

Throughout the tests, the parameters used in the algorithm are set as: $c_{att} = 0.35, c_{rep} = 8.2e-4, a = 0.32, b = 4$. And the grid size of OGM is chosen as $0.3 \times 0.3 \times 0.3$ m of cube.

Fig. 6 shows the result of one of autonomous swimming test. Here the green line indicates the path planning result and blue line means the vehicle trajectory. Start from point A, after recognize the total of 11 vision markers, the vehicle return to the end point. As mentioned before, from start point to point A, proposed FLS image processing based localization method is used for providing position aiding. Test result shows that this kind of localization method could provide satisfactory aiding information.

During the test shown in Fig. 6, we did not set any of obstacle. To demonstrate the obstacle detection and path planning algorithm presented in this paper, we carried out another test where we set a cylinder type of structure with the dimension of 2(L)x0.4(D)m. Obstacle detection and path planning result is shown in Fig. 7, where red circle indicates the detected obstacle.

From Figs. 6 and 7, we can see that the vehicle's trajectory is not quite smooth. Indeed, this is a sort of control problem. In fact, there is a tether cable connected between the vehicle and the surface unit such that we can monitor the vehicle motion in the water in real-time. For the convenience of cable handling, a quite number of buoyancy balls were mounted on the cable, especially near the terminal part connected to the vehicle. This kind of tether cable might impose severe strain on the vehicle's pitch motion. On the other hand, for the test-bed vehicle, there are only two vertical

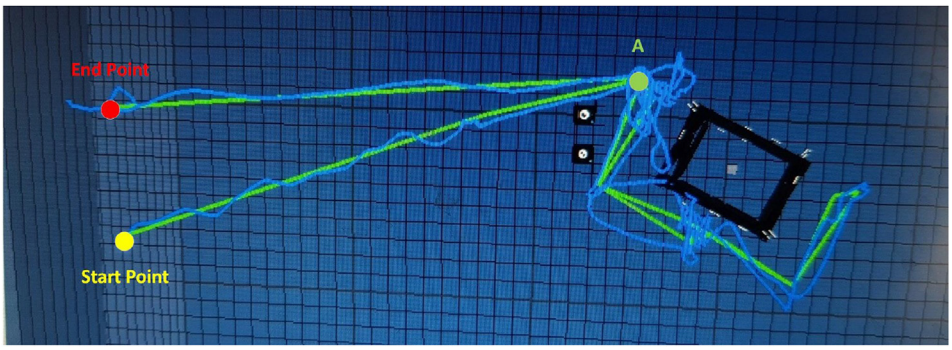

Fig. 6. Autonomous swimming test result.

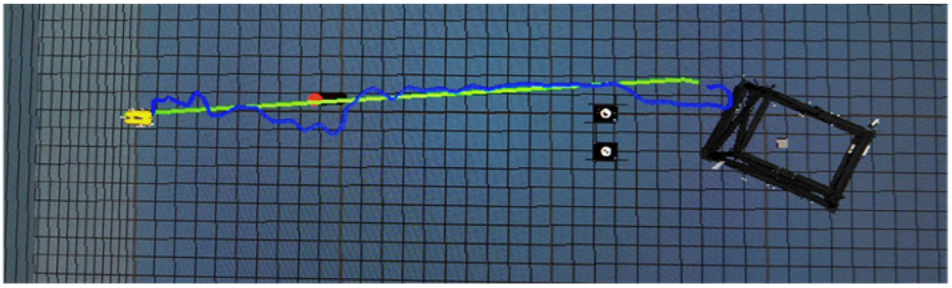

Fig. 7. Obstacle detection and path planning algorithm test.

thrusters, one is on the starboard and the other one on the port side (Li et al., 2017). All of these mechanical problems cause it difficult to stabilize the vehicle's pitch motion.

Finally, we carry out a fully autonomous swimming test. In this case, there is not tether cable or something other ropes connected between the vehicle and surface. This means the vehicle has to fully autonomously swim around and carry out the mission previously set to the vehicle on the surface. Fig. 8 shows the captured video clips taken by the diver who follow the vehicle throughout the test. During the test, the vehicle swims in and out of the structure and recognizes the full of 24 vision markers in sequence.

6. Conclusion

In this paper, we have presented an autonomous swimming technology developed for an AUV operating in the complicated underwater jacket structure environment. In case of the vehicle being far away from the structure(s) and therefore no artificial markers available for the vehicle to apply camera vision, a sort of FLS image processing based localization method has been proposed

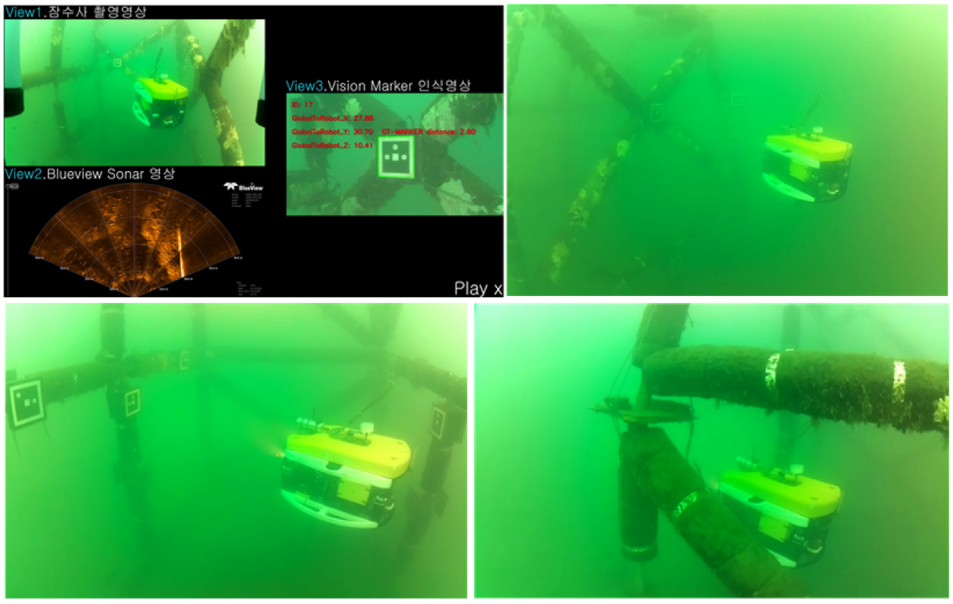

Fig. 8. Fully autonomous swimming test in the jacket structure environment.

for position aiding to the vehicle's hybrid inertial navigation system. Also, an OGM based obstacle detection and path planning algorithm has been discussed. In the case of local minimum, we can modify the coefficients values of potential function and reconstruct the OGM, and further re-search a path to the target point. This process will be repeated until we find out a path approaching to the target point. A series of experimental studies have been carried out in both of the water tank and the sea environment, and the test results show the effectiveness of presented localization and path planning algorithms.

Given the geometric information of the vehicle's operating field, we can construct the corresponding OGM where the 3D field is divided into connected grids pile and each grid is assigned an unique value calculated through certain potential function. For the grid size, if the size is too small, then we might need too long of both of OGM construction and search time. In contrast, if the grid is too large, then it might be impossible for us to find out accurate path for the vehicle to swim through the jacket structure. In some cases, according to the practical mission requirement, the grid size can be set differently in the same field in order to optimize the algorithm performance. How to choice the grid size in the practical applications might be one of most interesting issues in our future works.

Acknowledgement

This research was partially supported by the grant No. 10043928 from the Industrial Source Technology Development Programs of the MOTIE in the South Korea, and also supported by the project No. 17-CM-RB-16 titled “Development of Multi-sensor Fusion based AUV's Terminal Guidance and Docking Technology,” and funded by the Agency for Defense Development (ADD) in the South Korea.

References

BlueView Technologies Inc, 2013. ProViewer Sonar Development Kit User's Guide.
Fairfield, N., Kantor, G., Jonak, D., Wettergreen, D., 2008. DEPTHX Autonomy Software: Design and Field Results. Tech. Report CMU-RI-TR-08-09. Robotics Institute, Camegie Mellon University (July).
Farrell, J., Barth, B., 1998. The Global Positioning System and Inertial Navigation. McGraw-Hill.
Jung, J.D., Li, J.H., Choi, H.T., Myung, H., 2017. Localization of AUVs using visual information of underwater structures and artificial landmarks. Intell. Serv. Robot. 10, 67–76.
Latombe, J.C., 1991. Robot Motion Planning. Kluwer Academic Publishers, Massachusetts.
Laugier, C., Chatila, R., 2007. Autonomous Navigation in Dynamic Environments, first ed. Springer-Verlag Berlin, Heidelberg.
Lee, P.M., Jun, B.H., Kim, K.H., Lee, J.M., Aoki, T., Hyakudome, T., 2007. Simulation of an inertial navigation system with range aiding for an autonomous underwater vehicle. IEEE J. Ocean. Eng. 32 (2), 327–345.
Lee, Y.J., Choi, J.W., Ko, N.Y., Choi, H.T., 2017. Probability-based recognition framework for underwater landmarks using sonar images. Sensors 17 (9). https://doi.org/10.3390/s17091953.
Lewis, F.L., 1986. Optimal Estimation. John Wiley & Sons, Inc.
Li, J.H., Lee, M.J., Kim, J.G., Park, S.H., Suh, J.H., 2012. Guidance and control of P-SURO II hybrid AUV. In: Proceedings of MTS/IEEE Oceans'12 Yeosu 2012, Korea.
Li, J.H., Kang, H.J., Park, G.H., Ki, H.S., Suh, J.H., 2017. Sonar image processing based underwater localization method and its experimental studies. In: Proceedings of MTS/IEEE Oceans'17 Anchorage, Alaska.
Li, J.H., Park, D.G., Ki, H.S., 2018. Sonar image processing based underwater localization and path planning for AUV's autonomous swimming. In: Proceedings of 5th International Conference on Control. Decision and Information Technologies, Thessaloniki, Greece, pp. 611–615.
Russell, S.J., Norvig, P., 2009. Artificial Intelligence: A Modern Approach, third ed. Prentice Hall, Upper Saddle River, New Jersey.
Thurn, S., Burgard, W., Fox, D., 1997. Probabilistic Robotics. The MIT Press.
Tittertonm, D.H., Weston, J.H., 1997. Strapdown Inertial Navigation Technology. Peter Peregrimus Ltd., UK.